New Journal of Physics
The open-access journal for physics

Quantum size effects on surfaces without a projected bandgap: Pb/Ni(111)

Tjeerd R J Bollmann, Raoul van Gastel, Harold J W Zandvliet and Bene Poelsema[1]

Physics of Interfaces and Nanomaterials, MESA$^+$ Institute for Nanotechnology, University of Twente, PO Box 217, NL-7500AE Enschede, The Netherlands
E-mail: b.poelsema@tnw.utwente.nl

New Journal of Physics **13** (2011) 103025 (16pp)
Received 1 July 2011
Published 20 October 2011
Online at http://www.njp.org/
doi:10.1088/1367-2630/13/10/103025

Abstract. We have studied the initial growth of Pb on Ni(111) using low-energy electron microscopy (LEEM) and selective area low-energy electron diffraction (μLEED). First, a one-layer-high wetting layer develops that consists of small (7×7) and (4×4) domains. For larger coverages, Pb mesas are formed that are embedded in the wetting layer. In spite of the absence of a projected bandgap on clean Ni(111), we observe distinct quantum size effect (QSE)-driven preferred heights. These are apparent from a variety of frequently occurring island height transitions during growth, both on wide terraces and across substrate steps. Also, the average island heights that evolve during deposition at 422 and 474 K show a clear signature of QSE-driven preferred heights. These distinctly include five, seven and nine layers and thus correspond nicely to the values obtained in the key examples of QSE: Pb films on Si(111) and Ge(111). We suggest that the Pb-induced surface modification of Ni(111) shifts the Fermi level into the gap of the interface projected Ni bulk bands, thereby effectively causing decoupling of the Pb states with the bulk Ni states.

[1] Author to whom any correspondence should be addressed.

Contents

1. Introduction

With their low surface free energy, Pb films tend to wet most surfaces. However, quantum size effects (QSE) often result in distinct preferred heights for isolated Pb islands [1]. Recently, the self-organization into these island heights due to QSE, referred to as quantum growth or electronic growth, was observed on different substrates and was characterized with a variety of techniques [2–5]. A prototypical example of QSE is provided by thin Pb(111) films. For Pb with $d \approx 0.75\lambda_F$, with d being the interlayer distance and λ_F the Fermi wavelength, every increment by two layers almost perfectly accommodates three additional antinodes of the Fermi wavefunction. Recently, many intriguing features were discussed for the growth of Pb on Si(111) [2], [6–9], where flat top Pb islands with steep edges grow to specific integer heights that are stabilized by QSE. It was shown that Pb mesas grown on both Si(111) and Ge(111) are atomically smooth at substrate temperatures in the range of 200–300 K. The growth shows a strong preference for a bilayer increment in height on the top of a wetting layer, which is thought to passivate the substrate. The stable thicknesses found for Pb/Si(111) are initially odd layer heights 5, 7, 9, 11 and 13, crossing over to even layer heights 14, 16, 18, 20 and 22 thick *on top* of the wetting layer. The crossing from preferred odd to even island heights and vice versa shows a long 9.5 layer beating pattern as a result of the slight incommensurability of the Fermi wavelength to the interlayer distance [10, 11].

Typically, for QSE to manifest themselves quantum well states have to form in the metallic overlayer. This is, for instance, the case for Cu(111) and Ag(111), in contrast to Ni(111) [12]. Indeed, Pb layers on Cu(111) show strong evidence for the presence of quantum well states [4, 13]. Closer inspection of the calculations of Goldmann *et al* [12] reveals that the projected band structure obtained for the clean Ni(111) resembles Cu(111) and Ag(111). At the Γ point, the projected bulk band maximum is only 0.2 eV above the Fermi level and the crystal-derived surface bands are in close vicinity to it. Therefore, Ni(111) is an interesting candidate to investigate whether an interface projected band gap develops upon deposition of Pb, thereby facilitating quantum well states in thin Pb films.

Here, we present a study of the growth of thin Pb films and islands on the Ni(111) substrate and their subsequent temporal evolution as a result of QSE-driven growth. Using *in situ* low-energy electron microscopy (LEEM) and selected area low-energy electron diffraction (μLEED), we are able to probe the properties of different selected microscopic sample areas in real time. Using LEEM, we are also able to measure the island height evolution

during growth, thereby revealing electronic growth-driven transitions of Pb islands. Using μLEED we are able to probe the ordering of the Pb films and determine their structural properties.

2. Methods

The experiments were performed in an Elmitec LEEM III instrument. A Ni(111) surface was cleaned by successive cycles of 1 keV Ar^+ bombardment at room temperature (RT), followed by flash annealing to a temperature of 1150 K. The cleanness of the sample was monitored by Auger electron spectroscopy and LEEM. LEEM images revealed terraces with a width of $\sim$1 μm. All sample temperatures are subject to an uncertainty of 5% and were calibrated using the uphill motion of steps over time at a temperature where sublimation is observed, as described in [14]. Lead was deposited from a Knudsen cell. According to the bulk phase diagram, lead and nickel are immiscible in the bulk [15]. The typical deposition rate used in the experiments was about 1×10^{-3} ML s^{-1}, where a coverage of $\theta_{Pb/Ni} = 1$ ML corresponds to one Pb atom per Ni surface atom.

3. Results and discussion

3.1. Wetting layer properties

To determine the properties of a single Pb layer on top of the Ni(111) surface, we performed μLEED, illuminating a circular area of 19 μm diameter. When depositing Pb on the clean Ni(111) surface at a temperature of 474 K, we found a faint $(\sqrt{3}\times\sqrt{3})$-R30° surface alloy peak emerging, showing its maximum peak intensity at a coverage of 0.33 ML, corresponding to 250 s of deposition (see figure 1). The measured deposition rate is therefore 1.3×10^{-3} Pb atoms per unit cell (uc) per second (Pb/uc/s). The $(\sqrt{3}\times\sqrt{3})$-R30° surface alloy was also found in the literature, where annealing to $T > 850$ K followed deposition at RT before alloy formation occurred [16–19]. A further increase in coverage results in dealloying and the formation of a Pb wetting layer that covers the entire surface above $\theta_{Pb/Ni} \approx 0.40$ ML. From this coverage onward, new diffraction peaks emerge at a position corresponding to an in-plane lattice constant of 3.93 Å, giving rise to a weak moiré pattern. These Pb peaks move outward with increasing coverage, indicating a continuous compression of the aligned and incommensurate hexagonal Pb layer. The coverage in this wetting layer increases both as a result of the addition of Pb from the gas phase and due to continuous dealloying. The rate of dealloying increases with coverage, as can be concluded from the convex shape of the in-plane lattice constant versus coverage curve in figure 2(a). The wetting layer is completed when the compression of the in-plane lattice constant ends abruptly at a value of 3.50 Å. At this point the dealloying and the compression stop. This provides an excellent opportunity for an exact *in situ* calibration of the deposition rate. The resulting deposition rate is 1.33×10^{-3} ML s^{-1}, in agreement with the value obtained from the maximum peak intensity of the $(\sqrt{3} \times \sqrt{3})$-R30° surface alloy. We find no indication of the locking-in of the previously reported (3×3) structure found at RT [16, 18, 19], at an in-plane lattice constant of 3.73 Å.

Beyond a coverage of $\theta_{Pb/Ni} = 0.51$ ML, the line profiles shown as insets in figure 2(a) exhibit an unexpected peak splitting. The splitting reveals two different domains in the wetting layer, as illustrated by the μLEED pattern. These two domains are the (7×7) and (4×4)

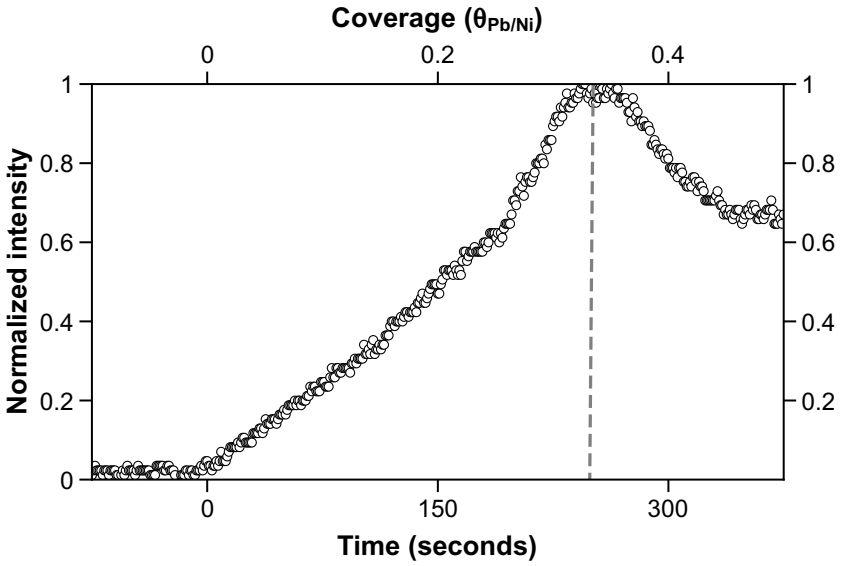

Figure 1. Integrated spot intensity for the $(\frac{1}{3}, \frac{1}{3})$ surface alloy diffraction peaks. The shutter was opened at $t = 0$ s. The maximum at $\theta_{\mathrm{Pb/Ni}} = 0.33$ ML is used for the *in situ* calibration of the deposition rate.

structures with lattice constants of 3.50 and 3.32 Å. Both have been reported on in the literature [16, 19] and are illustrated in figures 2(b) and (c). For increasing coverage the main spot intensity moves gradually from the less dense (7×7) domains at $\theta_{\mathrm{Pb/Ni}} \approx 0.51$ ML to the denser (4×4) domains at $\theta_{\mathrm{Pb/Ni}} \approx 0.55$ ML, as is reflected in the line profiles shown as insets in figure 2(a). This remarkable two-domain structure of the wetting layer was not anticipated and is found to disappear at 520–525 K, resulting in the anomalous transition of Pb mesas into hemispheres [20]. With the nearest-neighbor distance in bulk lead being 3.50 Å and the known generic tendency for tensile surface stress [21], we suggest that the (7×7) domains in the wetting layer involve tensile stress. A slight compression then locks the (4×4) domains.

To discuss the stability of both domains, we perform a coordination analysis. As a measure of the coordination of an individual Pb atom we take the sum of the lateral components of its position vector, measured along the directions of the three nearest Ni atoms underneath, relative to those values for an atom in a hollow site. For an on-top site, bridge site and threefold hollow site, we found a value of 1.734, 0.444 and 0, respectively, expressed in Ni lattice constants. The average numbers for the (7×7) and (4×4) structures are 0.550 and 0.618, respectively. This clearly suggests that the coordination is higher, and thus the binding stronger, for the (7×7) structure than for the (4×4) structure, in line with our observations. The strong binding to the Ni(111) substrate results in the accumulation of lateral stress, forcing the system to relieve this by keeping the compressed (4×4) domains small and alternating them with low-tensile-stress (7×7) domains. These Pb domains with different surface stresses can give rise to self-assembly [22]. A typical example is the striped phase formation of Pb on Cu(111) driven by competition between tensile and compressive stresses of a PbCu surface alloy and a Pb overlayer phase [23]. Here, the energy involved in the creation of the domain walls is low due to the alignment to the Ni substrate and the similar atomic densities of the (7×7) and (4×4) domains. This results in small domains with probably fast fluctuations. These domains are not

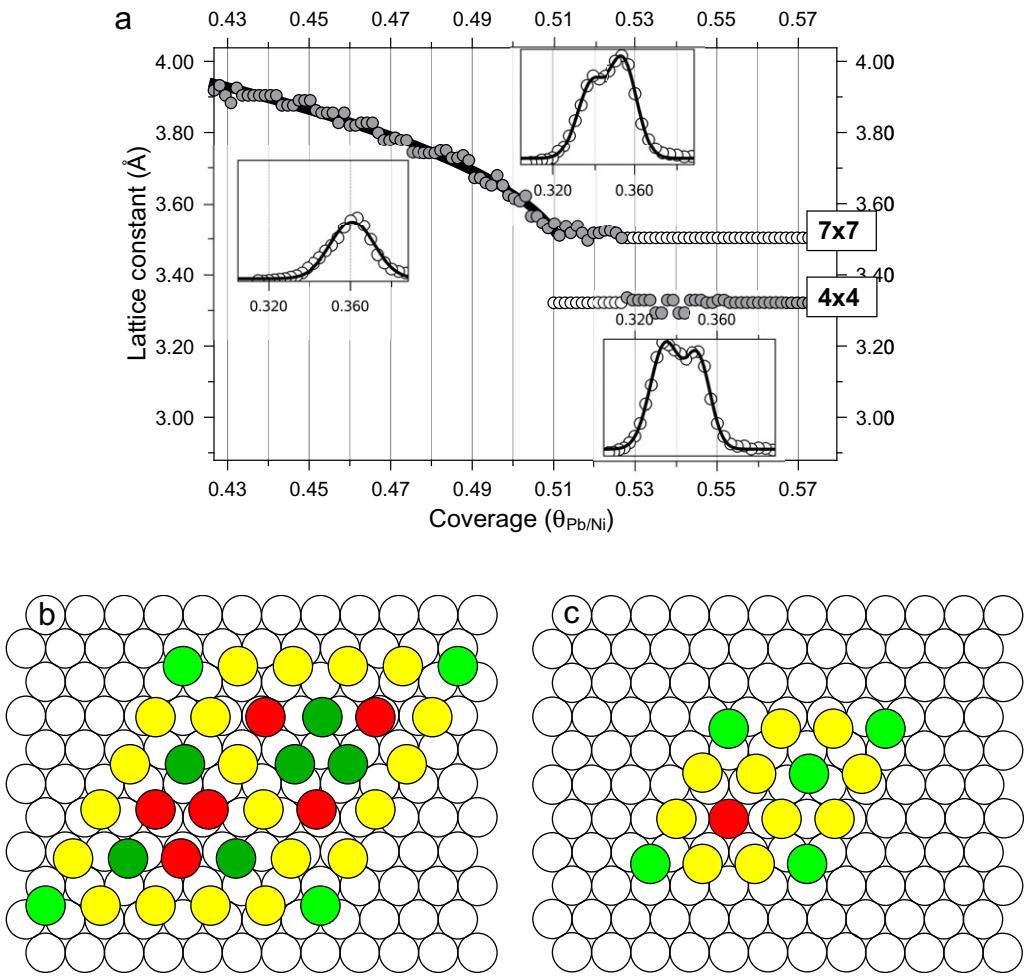

Figure 2. (a) The in-plane lattice constant as derived from the position of the Pb(1,0)-LEED spot (35.0 eV) during Pb deposition at 474 K. Snapshots of the corresponding peak line profiles are shown for the three different regions, as described in the text. The in-plane lattice constant of 3.50 Å corresponds to the (7×7) structure of the wetting layer with a coverage of 0.510 ML, where the in-plane lattice constant of 3.32 Å corresponds to the (4×4) structure of the wetting layer with a coverage of 0.563 ML. (b, c) The real-space unit cells for the (7×7) and (4×4) structures of the wetting layer, respectively. Green color (dark gray) corresponds to threefold hollow, darker green (darker gray) to close to threefold hollow, red (darkest) to (near) on-top and yellow (light gray) to intermediate positions.

resolved, probably because of the spatial resolution of our instrument of about 7 nm, possibly in combination with fast fluctuations at these temperatures.

For coverages $\theta_{\mathrm{Pb/Ni}} > 0.55$ ML, small Pb islands form. For these and all the other structures grown, μLEED shows only the bulk nearest-neighbor distance for completely relaxed Pb(111), coexisting with the strained double domain wetting layer. This observation is a consequence of the low misfit energy, which also allows for gradual in-plane lattice constant

compression of the incommensurate wetting layer, as shown in figure 2(a). The relatively low misfit energy is attributed to the large difference of atomic radii for Ni and Pb.

From here onwards, we define the coverage $\theta_{\mathrm{Pb}} = 1$ ML as the equivalent of one bulk Pb(111) layer.

3.2. Electronic growth-driven shape transitions of Pb islands

An eye-catching feature of the evolving morphology of the growing Pb film is the apparent difference of growth rates of individual islands. A significant fraction of the islands even appear to shrink in fractional area. These remarkable events occur both for islands far away from substrate steps and for those located at or in the close vicinity of substrate steps. They also occur during initial and more advanced stages of growth and are all explained in the context of QSE-driven stable island heights, as described in [24]. We consider them to be strong indications of the importance of QSE for Pb on Ni(111).

After completion of the wetting layer, Pb island nucleation is observed for coverages beyond $\theta_{\mathrm{Pb}} \approx 1.08$ ML, imaged as dark features in figures 3 and 4. The experiment shown in figures 3 and 4 is performed at a slightly lower temperature of 422 K. During the growth of these small islands, we observe the sudden collapse of their fractional area within a few seconds. In figures 3 and 4, two examples are shown. Island areas are measured by making use of common image analysis techniques such as background subtraction, Otsu's method to automatically perform histogram shape-based adaptive image thresholding [25] and standard erosion and dilation filters. Quite clearly, we can distinguish islands that undergo a reduction in fractional area between frames. The condition of mass conservation leads to the conclusion that the islands must undergo a height increase at the same time.

We first focus on the LEEM images in figure 3 (insets) and the corresponding cartoons below them. Going from image (a) to (b), taken only 7 s apart, we observe a distinct reduction in the fractional area of the highlighted island. This is exemplified by the plot of the fractional area against time in figure 3. The ratio of the final and the initial projected areas, A_5 and A_3, respectively, is $R_A = 0.50$. Since there is no mass transport between this island and any of its neighbors, and nor does any intensity fluctuation in its surroundings take place, mass conservation must apply. The reduction in area must therefore be accompanied by a corresponding increase in height; see figures 3(c) and (d). The wetting layer (gray) has an approximately 8% higher density than the completely relaxed Pb(111) layers in the islands. The height of the islands is counted with respect to the substrate. Assuming mass conservation, the following condition must apply: $3 \times A_3 = 5 \times A_5 + 1.08 \times (A_3 - A_5)$. This gives $R_A = \frac{A_3}{A_5} = 0.49$, i.e. the ratio R_A is identical to the measured value within the experimental uncertainties. The conclusion is that the transformation of the island is from a three-layer-high island into a five-layer-high island. Keeping in mind that the measurement takes place during the deposition of Pb, the growth rate of the islands must differ by a factor of 2. Indeed, this is nicely confirmed by the two-times higher expansion rate of the three-layer-high island compared to the five-layer-high one, as inferred from the measured slopes in figure 3. These findings provide strong support for the assessment of a transition from a three-layer-high island to an island with the preferred height of five layers. We attribute this bilayer height transition to QSE.

A similar feature is illustrated by the LEEM images in figure 4 (insets). Here we start with a larger island situated near a descending step in the Ni(111) substrate. The reduction of the fractional area of this island is plotted in figure 4. The transition occurs in a more complex

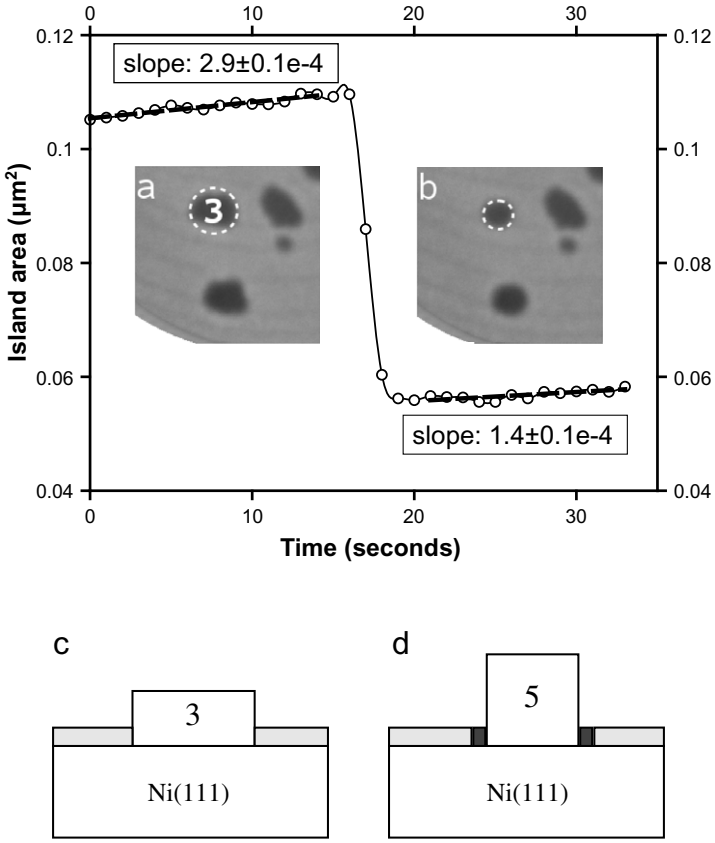

Figure 3. Plot of the island area of the island shown in the insets against time. Insets (a) and (b) show $1560 \times 1560\,\mathrm{nm}^2$ LEEM images recorded at an electron energy of 20.0 eV after deposition of $\theta_{\mathrm{Pb}} = 1.28$ ML at 422 K. (c, d) Cartoons of the shape transition.

way, but the overall result is a ratio of the final fractional area to the initial one of 0.75. For a transition from a four-layer-high island to a preferred five-layer-high island, shown in figures 4(c) and (d), mass conservation conditions imply $4 \times A_4 = 5 \times A_5 + 1.08 \times (A_4 - A_5)$, which gives $R_A = \frac{A_4}{A_5} = 0.74$, consistent with the experimental value within the experimental uncertainties. The scatter in the growth rate is in this case much larger, but again the obtained result of the final growth rate being 0.64 times smaller than the initial one is consistent with the expected factor of 2/3. So again, in this transition of the island we find strong evidence for a preferred island height of five layers. We conclude that the data in figures 3 and 4 demonstrate the importance of QSE in this system. Note that the growth rate of the island in figure 3 is two times larger than that found for the island in figure 4. This difference is attributed to the influence of substrate steps in the vicinity of the islands.

From the conservation of the total amount of deposited material and the observed height transitions, we can also derive that the Pb(111) islands grow directly on the metallic Ni(111) substrate and are surrounded by the wetting layer consisting of both (7×7) and (4×4) domains. This is in contrast to the wetting layer of Pb and Bi on Si(111), where the semiconducting substrate is first passivated by the wetting layer before electronic growth starts on top of it [10, 26, 27].

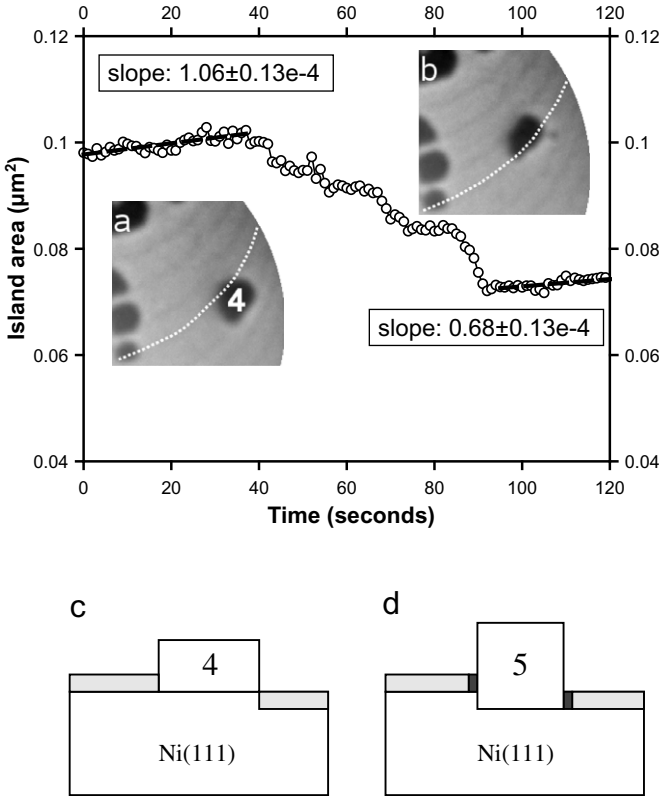

Figure 4. Plot of the island area of the island shown in the insets against time. Insets (a) and (b) show $1560 \times 1560\,\mathrm{nm}^2$ LEEM images recorded at an electron energy of 20.0 eV after deposition of $\theta_{\mathrm{Pb}} = 1.47$ ML at 422 K. The island traverses the substrate step that is in contact with the island, indicated by the dashed line, from 40–90 s. The interaction with the step slows the transition down (compare figure 3). (c, d) Cartoons of the shape transition.

After prolonged deposition at a slightly higher temperature of 474 K, islands can achieve large fractional areas. Adjacent islands can make concerted movements in an attempt to minimize their energy. Figures 5(a) and (b) show an example at an average film thickness of about 17.5 layers. A concerted movement across a step enables a height transition of one of the islands. The two islands taking part in this concerted movement are labeled by their contours in red (dark) and green (bright) and are assumed to initially have the same uniform height, h, composed of n layers. The Ni substrate step in between these islands is marked by the white dashed line. As a result of the net flow of Pb atoms from the green (bright) labeled island towards the red (dark) labeled island across the substrate step, both islands reduce their projected area, as shown in figures 5(a) and (b). The filled circles in the graph of figure 5(c) show the total measured fractional area times a constant height h. Assuming that both islands are initially smooth and thus have a uniform height, as well as assuming mass conservation, a height doubling of the red (dark) island results in the open circles in figure 5(c). This curve represents the fractional area multiplied by a time-dependent height $h(t)$ for the red (dark) labeled island, where $h(t)$ is a step function that is equal to h for $\theta_{\mathrm{Pb}} < 8.439$ ML and $2h$ for $\theta_{\mathrm{Pb}} \geqslant 8.439$ ML. The transition region, $\theta_{\mathrm{Pb}} = 8.439$–$8.447$ ML, shows that the atomic rearrangement takes less

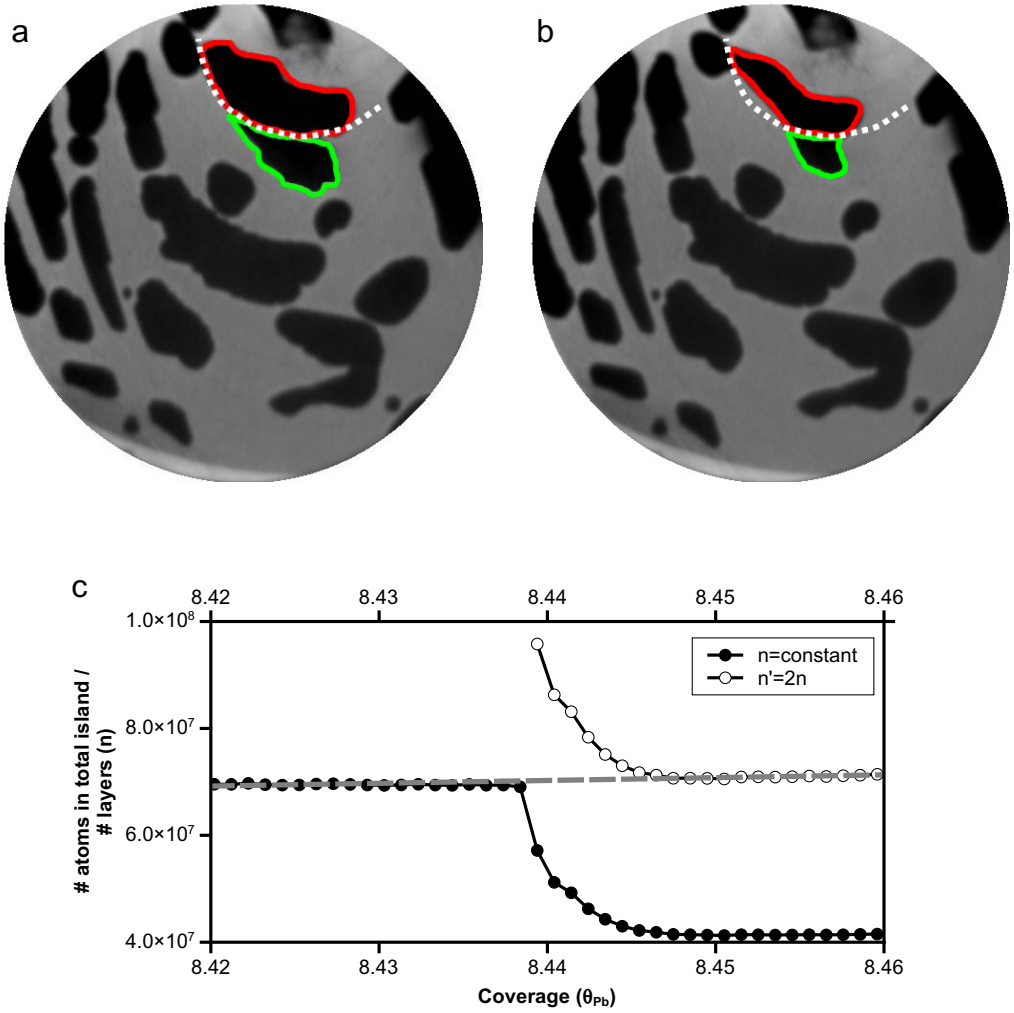

Figure 5. (a, b) LEEM images (FoV = 15 μm, the electron energy is 20.0 eV, $\theta_{Pb} = 8.42$ and 8.46 ML) showing concerted movement of the islands indicated by the red (dark) and the green (light) contour. The substrate step in between is drawn as a white dashed line. (c) Graph of the calculated number of island atoms divided by the number of layers (n). The decrease of fractional area in the case when n being constant is shown by filled circles. Assuming island height doubling ($n' = 2 \times n$) of the red (dark) island for $\theta_{Pb} \geqslant 8.439$ ML leads to conservation of the atoms contained in the island (open circles).

than 10 s. For the LEEM images shown in figures 5(a) and (b), the average island height, calculated from a total fractional island area of 47.7%, is about 17.5 atomic layers. It is therefore likely that the red (dark) island makes a transition from a layer height of, e.g., nine layers to 18 layers. From the literature, it is known that Pb(111) films are rather special in that the Friedel oscillations at their surface allow strong QSE to persist even over 30 atomic layers thickness [11]. The slight incommensurability of the Fermi wavelength to the interlayer distance results in periodic crossovers in the stability of odd versus even layer heights [24]. This provides strong support for the height transition of the red (dark) island from an odd layer height below

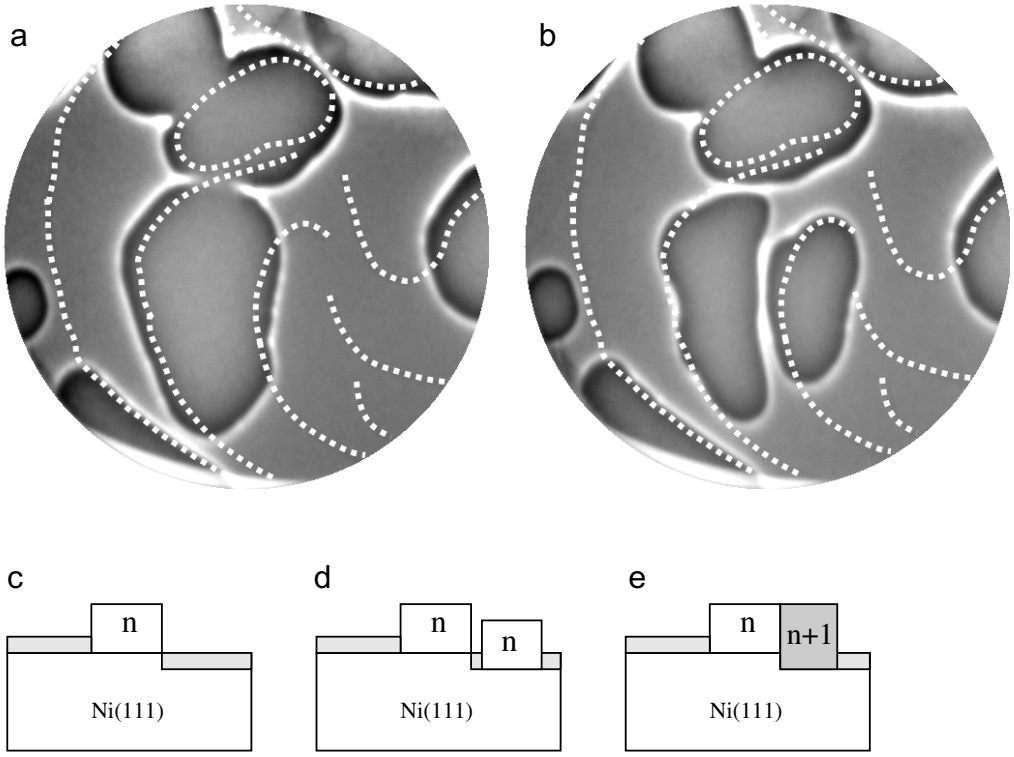

Figure 6. (a, b) LEEM images (FoV = 4 μm, the electron energy is 5.0 eV and $\theta_{Pb} = 4.57$ and 4.79 ML) showing the splitting of an island over a substrate step in order to regain an energetically favorable QSE stabilized height. The substrate steps are shown by white dashed lines. (c–e) Cartoons corresponding to the island splitting over a substrate step, where the final situation in (d) is stable according to the bilayer periodicity of stable island thicknesses. For the same reason, (e) is unstable.

11 (e.g. seven or nine) atomic layers, to an even layer height (e.g. 14 or 18). From average island height measurements, we also found stable island heights of seven and nine at 474 K, discussed below and visualized in figure 7. These are in agreement with the observation in figure 5 and the corresponding proposed height of less than 11 atomic layers. We note that a comparison of the growth rate of the resulting island with those found previously (see e.g. figure 4) is consistent with this assignment. We also note that the local free energy minima near the transition from odd to even crossover of preferred layer heights facilitate a pronounced instead of an incremental increase of the island height [10].

Figure 6 shows another example of the strong preference for specific QSE stabilized heights. In the center of the 4 μm wide image in figure 6(a), a QSE stabilized island has expanded its area up to the full terrace width, where the bounding steps are marked by white dashed lines. As soon as it extends slightly over the descending step, the height on the lower terrace becomes one atomic layer higher, which is energetically less favorable due to the bilayer periodicity of stable island thicknesses. Therefore, it becomes energetically more favorable for the island to split into two separate islands, one on each terrace with similar heights (see figures 6(c) and (d)), despite the creation of additional island boundaries. The average island height in figure 6, calculated from the islands' total fractional area, is about 15 layers. Since the

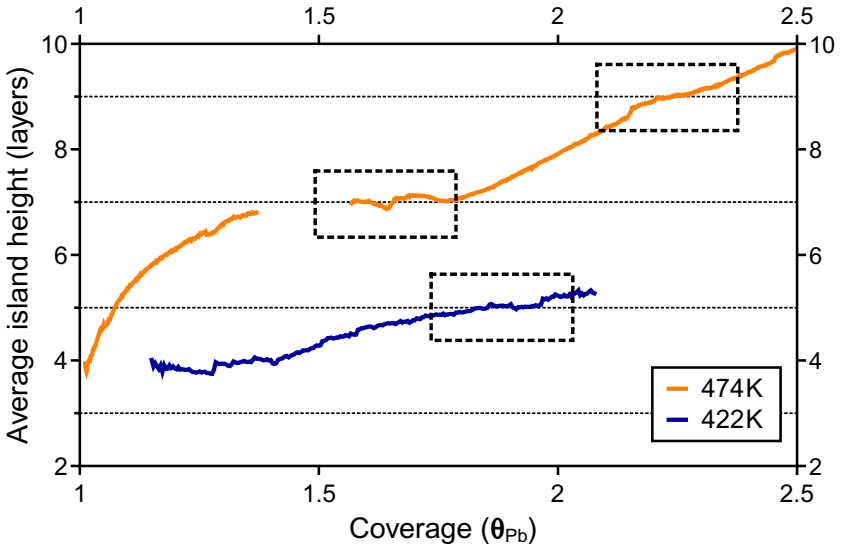

Figure 7. The average island height as a function of coverage for the temperatures of 422 and 474 K. Stable island thicknesses of five, seven and nine atomic layers were found.

heights of both islands are very similar, we are not able to assign exact island heights within the experimental error of the fractional area. 14- and 16-layer-high islands would be likely candidates.

In order to gather more dynamic and global information on the evolution of the island height, we measured the *average* island height for a large number of frames for coverages from $\theta_{Pb} = 1.0$–2.5 ML. In figure 7, such measurements are shown for temperatures of 422 and 474 K, where the island density for the latter is lower. From this figure, the tendency of both curves to flatten at five layers for 422 K, at seven layers, and less pronounced at nine layers for 474 K, is attributed to the strong preference for QSE stabilized island heights. Islands reach an energetically stable height and merely expand laterally. Keeping in mind that we consider average values for the island heights and that we are dealing with a distribution of island heights, we have to consider the tendency for a preferred height to be strong support for its existence. The measured QSE stabilized heights of five, seven and nine atomic layers show bilayer periodicity and are in agreement with the literature [10, 24, 28]. For the higher temperature of 474 K, the first stable height is seven atomic layers. At a slightly lower temperature the first stable height appears to be five atomic layers. However, we have clear evidence for the existence of three-layer-high islands (see above). From the fact that the curve for the 422 K data starts at four layers for $\theta_{Pb} = 1.0$ ML, where exact data are missing up to $\theta_{Pb} = 1.15$ ML due to re-adjustment of the instrument, we are probably dealing with a mixture of both three- and five-layer-high islands. The first are metastable at this temperature. Consequently, these data may provide the first experimental evidence for preferred three-layer-high islands in electronic growth of Pb films, as predicted by theory [10, 28]. The 'noise' at the start of the 422 K data can actually be traced back to transitions from three to five layers and is by no means just a statistical feature. For increasing coverage, the spread in island heights increases and therefore the flattening in figure 7 becomes less pronounced.

Table 1 summarizes the observed stable heights in our experiments in comparison to those found for Pb on Ge(111) and Si(111) [3, 29]. Note that the growth of QSE-driven Pb

Table 1. A summary of the observed stable heights found for Pb films *on top* of the Ni(111) substrate; 's' stands for stable and 'u' for unstable. For comparison, the experimental observed stable heights for Pb films *on top of a wetting layer* on Ge(111) and Si(111) are shown; data are taken from [10]. See also figures 3–5.

Film thickness (layers)	2	3	4	5	6	7	8	9	10	11
Ni(111)	u	s	u	s	u	s	u	s	–	–
Ge(111) ($\sqrt{(3)}\times\sqrt{(3)}$)-$\alpha$ [10]	–	–	–	s	u	s	u	s	u	s
Si(111) (7×7)-Pb [10]	–	–	–	s	u	s	u	s	u	s
Si(111) ($\sqrt{(3)}\times\sqrt{(3)}$)-$\alpha$ [10]	–	–	–	s	u	s	u	s	u	s

islands occurs *on top* of the wetting layer for Pb/Ge(111) and Pb/Si(111), where in the case of Pb/Ni(111) the islands grow directly on the bare substrate.

3.3. I/V-LEEM interpretation

We have discussed the electronic growth observations of Pb on Ni(111) using the morphological changes in our LEEM observations. We now focus on the interpretation of the I/V-LEEM curves obtained from the Pb islands. By varying the incident electron energy while measuring the reflected intensity, I/V-LEEM curves of the $(0,0)$ beam at normal incidence can be obtained. Typically, these I/V-LEEM curves exhibit pronounced quantum interference peaks, resulting from the QSE. The positions of these peaks can be easily predicted by a simple Kronig–Penney (KP) model; see [30] for a full description. In short: the KP model uses two potential boxes for each layer, with depth V and width w, centered at the atoms (V_a, w_a) and in between the atoms (V_g, w_g). The substrate is given as a featureless box with depth V_{0s}. By requiring the wave functions and their first derivatives to be continuous at the various transitions, including the vacuum–film interface, we can derive the reflection coefficient at the latter interface, which represents the measured quantity. The result is $N-1$ interference peaks for an N-layer-thick film. Analogous to the Pb on Ni(111) system, these predicted interference peaks were also found for the electronic growth of Bi on Ni(111) for island heights of three and five atomic layers [31].

Figure 8(a) shows the measured I/V-LEEM curves for a five-atomic-layer-high island, where the height is determined with an evaluation scheme similar to the one used in figures 3 and 4. A small but distinct quantum interference peak can be found at 3.5 and 11.9 eV, marked by arrows. The peak intensity of the quantum interference peaks (I_{QSE}) is rather small in comparison to the Bragg peak intensity (I_{Bragg}) around 22.0 eV, marked 'B' in figures 8(a) and (b), with a typical ratio of $\frac{I_{Bragg}}{I_{QSE}} \approx 20$. The S/N ratio is limited by the available intensity.

In order to qualitatively understand the distinct interference peaks in figure 8(a) we propose a simple KP model. Since no parameters for the Pb on Ni(111) system are known to the best of our knowledge, the parameters are based on the best fit parameters for a five-layer-high Bi island on Ni(111) [31] (see table 2). Using these values, we are able to qualitatively reproduce the experimental I/V-LEEM data (see figures 8(a) and (b)) with the exception of the intense peak at 7 eV. To fit the Bragg peak to the experimental data we use an interlayer distance, $w_a + w_g$, of 3.05 Å. This corresponds to a surface relaxation of almost 7% compared to bulk Pb. Large relaxations for the (four) outermost Pb(111) layers, larger than typically found for other fcc(111)

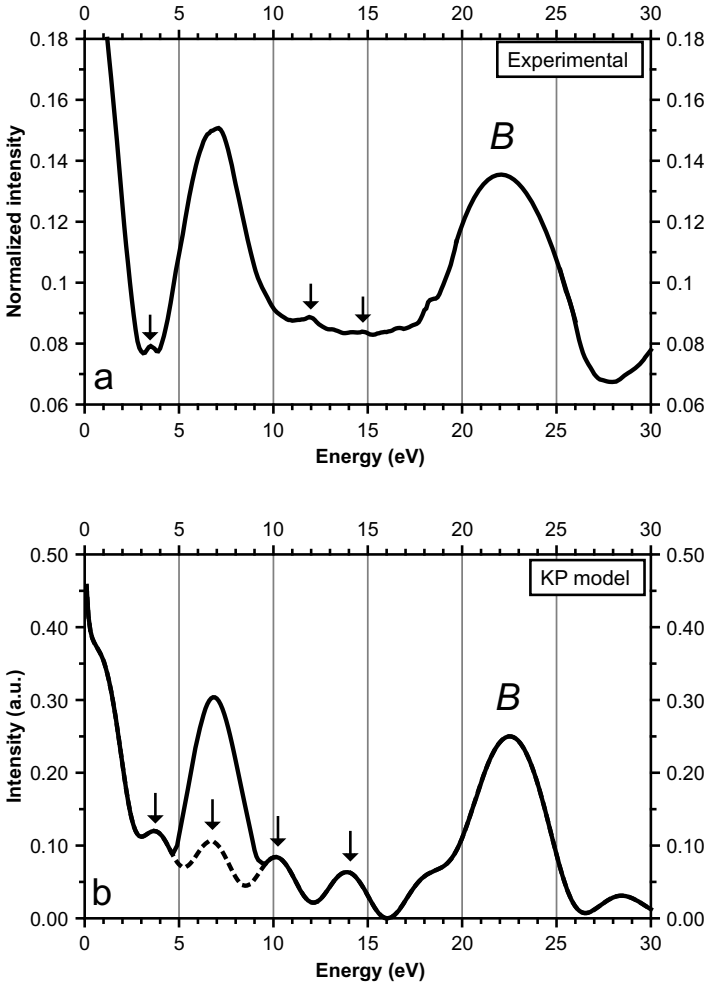

Figure 8. (a) Measured I/V-LEEM curve for a five-layer-high Pb island on Ni(111) at 474 K, $\theta_{\mathrm{Pb}} = 1.25$ ML. (b) Calculated I/V-LEEM curve based on the KP model using the parameters shown in table 2. For the dashed region, the addition of a parabola representing the band structure interference peak centered at 7 eV gives qualitative agreement with the measured curve. The arrows indicate the positions of the $N-1$ quantum interference peaks.

surfaces, are known to dominate at temperatures over $0.5T_{\mathrm{m}}$ [32], where bilayer modulations of the interlayer distance are also reported [33]. The large surface relaxations found for Pb(111) cause the quantum interference peaks to broaden and thereby reduce their peak height. We show that the positions of the quantum interference peaks at energies of 3.7, 10.2 and 18.1 eV are in qualitative agreement with the experimental I/V-LEEM curve. The intensity ratio between the Bragg peak and the quantum interference peak at 3.7 eV for the KP model is about $\frac{I_{\mathrm{Bragg}}}{I_{\mathrm{QSE}}} = 10$. The higher ratio for the measured curve may well be explained by the peak broadening, along with the Debye–Waller factor and/or dynamic effects.

The intense peak at 7 eV in figure 8(a) is attributed to band structure effects. From the literature it is known that sharp peaks in reflectance correlate with band structure crossings and gaps along the ΓL line of the Brillouin zone [34]. Typically for fcc metals, these sharp peaks

Table 2. The parameters used for the KP model shown in figure 8(a). The values are based on [31].

Parameter	V_a (eV)	V_g (eV)	V_{0s} (eV)	w_a (Å)	w_g (Å)
Value	20.7	10.2	20.0	1.35	1.70

lie near the Γ_2' point or Γ_7^- in double group notation [35]. The position of Γ_2' at 10 eV above E_F [36] correlates with the intense peak at 7 eV after the addition of the inner potential [37] and the subtraction of the work function difference between the LaB_6 cathode [38] and thin Pb(111) films [9, 39]. Taking into account this band structure effect, we superimposed a peak at 7.0 eV in the KP model, shown by the solid line in figure 8(a) in the energy range of 4.6–9.5 eV. This results in qualitative good agreement with the measured I/V-LEEM curve in figure 8(a). Therefore, we conclude that the weak quantum interference peaks in the I/V-LEEM curve are also dominated by strong band structure effects around 7 eV.

We have demonstrated a wide variety of mostly circumstantial evidence for the occurrence of QSE in thin Pb layers on Ni(111). All features show a close resemblance to previous observations obtained for Pb on Cu(111) [13] and even on Si(111) and Ge(111) [10, 28]. Therefore, we can safely conclude that QSE are present in thin Pb films on Ni(111) and govern the film morphology. For an explanation of the decoupling of the Pb states with the Ni bulk bands, see [16] in which the authors report a work function reduction of not less than 0.7 eV for Pb-modified Ni(111). This directly results in a clear band gap in the interface projected Ni bulk bands with the Fermi level about 0.5 eV above the band maximum in the Γ point. In this situation, we fulfill all the requirements for observing QSE in Pb/Ni(111) as experimentally observed.

4. Summary

We have studied the growth and properties of thin Pb films on Ni(111). First, a one-layer-high wetting layer develops that consists of small (7×7) and (4×4) domains, where the former has a stronger binding to the Ni(111) substrate. This results in the accumulation of tensile lateral stress, forcing the system to relieve this by allowing the growth of compressively stressed (4×4) domains. Since the density in both domains is very similar and their azimuthal orientation is identical, the domain wall energy will be low. These low-energy cost domain walls result in small domain sizes.

For coverages $\theta_{Pb/Ni} > 0.55$ ML, Pb mesas form, which are embedded in the wetting layer. We have shown distinct QSE-driven preferred heights for the Pb mesas in a number of specific examples for relatively thin and thick films. This is apparent from island height transitions both on wide terraces and at substrate steps. The average island heights that evolve during deposition at 422 and 474 K show a clear signature of QSE-driven preferred heights, distinctly including stable heights of five, seven and nine atomic layers.

All features closely resemble previous observations for Pb films on Cu(111) as well as on Si(111) and Ge(111) [10, 13, 28]. The identified QSE in Pb/Ni(111) are attributed to Pb-induced modifications of the Ni(111) interface, leading to a band gap in the interface projected Ni bulk bands.

Weak quantum interference has also been identified in I/V-LEEM measurements. The experimental I/V-LEEM curve is also dominated by strong band structure effects around 7 eV.

Acknowledgment

This work was carried out as part of the research program of the Foundation for Fundamental Research on Matter, which is financially supported by the Netherlands Organization for Scientific Research.

References

[1] Zhang Z, Niu Q and Shih C K 1998 *Phys. Rev. Lett.* **80** 5381–4
[2] Binz S M, Hupalo M and Tringides M C 2009 *J. Appl. Phys.* **105** 094307
[3] Budde K, Abram E, Yeh V and Tringides M C 2000 *Phys. Rev.* B **61** R10602–5
[4] Hinch B J, Koziol C, Toennies J P and Zhang G 1989 *Europhys. Lett.* **10** 341
[5] Man K L, Qiu Z Q and Altman M S 2010 *Phys. Rev.* B **81** 045426
[6] Li M, Wang C Z, Evans J W, Hupalo M, Tringides M C and Ho K M 2009 *Phys. Rev.* B **79** 113404
[7] Man K L, Tringides M C, Loy M M T and Altman M S 2008 *Phys. Rev. Lett.* **101** 226102
[8] Binz S M, Hupalo M and Tringides M C 2008 *Phys. Rev.* B **78** 193407
[9] Wei C M and Chou M Y 2002 *Phys. Rev.* B **66** 233408
[10] Özer M M, Jia Y, Wu B, Zhang Z Y and Weitering H H 2005 *Phys. Rev.* B **72** 113409
[11] Jia Y, Wu B, Li C, Einstein T L, Weitering H H and Zhang Z 2010 *Phys. Rev. Lett.* **105** 066101
[12] Goldmann A, Dose V and Borstel G 1985 *Phys. Rev.* B **32** 1971–80
[13] Otero R, Vázquez de Parga A L and Miranda R 2002 *Phys. Rev.* B **66** 115401
[14] Ondrejcek M, Rajappan M, Swiech W and Flynn C P 2006 *Phys. Rev.* B **73** 035418
[15] Okamoto H 1991 *Binary Alloy Phase Diagrams* (Materials Park, OH: ASM)
[16] Gürtler K and Jacobi K 1983 *Surf. Sci.* **134** 309–28
[17] Umezawa K, Nakanishi S, Yumura T, Gibson W M, Watanabe M, Kido Y, Yamamoto S, Aoki Y and Naramoto H 1997 *Phys. Rev.* B **56** 10585–9
[18] Brown D, Quinn P D, Woodruff D P, Bailey P and Noakes T C Q 2000 *Phys. Rev.* B **61** 7706–15
[19] Krupski A and Mróz S 2003 *Surf. Rev. Lett.* **10** 843–8
[20] Bollmann T R J, van Gastel R, Zandvliet H J W and Poelsema B 2011 *Phys. Rev. Lett.* **107** 136103
[21] Dodson B W 1988 *Phys. Rev. Lett.* **60** 2288–91
[22] Marchenko V I 1981 *JETP Lett.* **33** 381
[23] Plass R, Bartelt N C and Kellogg G L 2002 *J. Phys.: Condens. Matter* **14** 4227–40
[24] Özer M M, Wang C Z, Zhang Z and Weitering H H 2009 *J. Low Temp. Phys.* **157** 221–51
[25] Otsu N 1979 *IEEE Trans. Syst. Man Cybern.* **9** 62–6
[26] Nagao T, Doi T, Sekiguchi T and Hasegawa S 2000 *Japan. J. Appl. Phys.* **39** 4567–70
[27] Hirahara T, Nagao T, Matsuda I, Bihlmayer G, Chulkov E V, Koroteev Yu M and Hasegawa S 2007 *Phys. Rev.* B **75** 035422
[28] Jia Y, Wu B, Weitering H H and Zhang Z 2006 *Phys. Rev.* B **74** 035433
[29] Özer M M, Jia Y, Zhang Z, Thompson J R and Weitering H H 2007 *Science* **316** 1594–7
[30] Altman M S, Chung W F and Liu C H 1998 *Surf. Rev. Lett.* **5** 1129–41
[31] Bollmann T R J, van Gastel R, Zandvliet H J W and Poelsema B 2011 *Phys. Rev. Lett.* **107** 176102
[32] Pussi K, Vuorinen J, Lindroos M, Li H I, Howe J D, Hanna K J, Diehl R D and Bandyopadhyay P K 2009 *Surf. Sci.* **603** 2759–63
[33] Mans A, Dil J H, Ettema A R H F and Weitering H H 2005 *Phys. Rev.* B **72** 155442

[34] Bartos I, Van Hove M A, Chung W F, He Z and Altman M S 1998 *Surf. Sci.* **402–404** 697–700
[35] Jaklevic R C and Davis L C 1982 *Phys. Rev.* B **26** 5391–7
[36] Horn K, Reihl B, Zartner A, Eastman D E, Hermann K and Noffke J 1984 *Phys. Rev.* B **30** 1711–9
[37] Li Y S, Jona F and Marcus P M 1991 *Phys. Rev.* B **43** 6337–41
[38] Yamauchi H, Takagi K, Yuito I and Kawabe U 1976 *Appl. Phys. Lett.* **29** 638–40
[39] Qi Y, Ma X, Jiang P, Ji S, Fu Y, Jia J F, Xue Q K and Zhang S B 2007 *Appl. Phys. Lett.* **90** 013109